Gezira J. of Engineering and Applied Sciences
ISSN Linking:
http://journals.uofg.edu.sd/index.php/gjeas/

Modeling Malaria Transmission and Control: An SIR–SI Framework with Three Optimal Intervention Strategies

Mojeeb AL-Rahman EL-Nor Osman, Mohammed Salaheddin Abdelkader[*].

[1]Department of Mathematics and Computer Science, Faculty of Pure and Applied Sciences, International University of Africa, P.O. Box 2469, Khartoum, Sudan.

[2]College of Commerce and Business, Lusail University, Lusail, Qatar.

[3]Department of Mathematics, Faculty of Mathematical and Computer Sciences, University of Gezira, Wad Madani, Sudan.

[4]Department of Mathematical Sciences, Collage of Sciences, United Arab Emirates University, P.O. Box 15551, Al Ain, UAE.

**Corresponding author email: mhmsalah@uaeu.ac.ae*

INFORMATION:

Submission:22/02/2026

Accepted:16/07/2026

Publication: 23/08/2026

ABSTRACT

In this study, we developed and analyzed an SIR–SI malaria transmission model that accounted for partial immunity and re-infection within recovered human population. The basic reproduction number, R_0, was obtained via the next-generation matrix approach, and the local as well as global stability of the disease-free equilibrium (DFE) were investigated. Both analytical and numerical analyses demonstrated the occurrence of a backward bifurcation, whereby a stable DFE could coexist with a stable endemic equilibrium under certain parameter conditions. Numerical simulations validated the theoretical results and further examined the effects of three time-dependent optimal control strategies: bed-net usage $u_1(t)$, antimalarial treatment $u_2(t)$, and insecticide spraying $u_3(t)$. Sensitivity analysis identified the human-to-mosquito transmission rate as a critical parameter influencing R_0. Model parameters describing mosquito biting behavior, natural mortality, and transmission rates were taken from published entomological and demographic sources, while the immunity-loss rate, recovery rate, and re-infection probability were estimated by fitting the model to WHO-reported cumulative malaria case data for the Democratic Republic of Congo, so the model was calibrated to regional epidemiological data rather than purely hypothetical. Simulation outcomes indicate that the integrated application of all three interventions yields the most significant and sustained reductions in human and mosquito infection prevalence, with the potential for disease eradication within a few years. These findings underscore the necessity of coordinated, multi-faceted intervention strategies for effective malaria control in high-burden regions, such as the Democratic Republic of Congo.

KEYWORDS: malaria transmission; stability analysis; bifurcation; numerical simulation; optimal control strategies**.**

1. INTRODUCTION

A. Background

Malaria is an infectious disease transmitted by the bite of infected female Anopheles mosquitoes. In 2022, the most recent report from the World Health Organization (WHO) estimated approximately 229 million cases and 409,000 deaths worldwide. The Democratic Republic of Congo (DRC) accounted for 12% of the global cases and 11% of the deaths, ranking second globally after Nigeria [1]. In 2022, sub-Saharan Africa accounted for about 95% of all cases and 96% of all malaria deaths, with about 80% of these deaths reported in children under the age of five years [2]. In 2023, across 33 moderate- to high-transmission countries in the WHO African Region, an estimated 36 million pregnancies occurred, of which 12.4 million (34%) were affected by malaria [3]. In 2021, the DRC was among the top contributors to the global malaria burden [4].

A. Mathematical Models for Malaria

Mathematical models serve as essential tools for understanding the dynamics of vector-borne diseases such as malaria. Since the introduction of the first mathematical model by Ronald Ross, extensive research has been conducted on modeling malaria transmission to gain deeper insights into its spread and control (Eikenberry and Gumel, 2018) [5]. Raj, et al, present a novel framework for modeling malaria transmission dynamics by integrating temperature and altitude dependent transmission functions into a compartmental SIR-SI model, 2025 [6]. Edoardo Beretta, et al, 2018, analyzed a mathematical model for malaria transmission that incorporates asymptomatic carriers within two distinct age groups of the human population. Their analysis identified key parameters—such as the mosquito biting rate and the mosquito mortality rate—as critical in determining disease dynamics. A threshold value, R_0, was derived based on these parameters. The results indicate that when $R_0 > 1$, an endemic equilibrium exists, whereas when $R_0 < 1$, the disease tends to die out [7]. Xiaomei Feng, et al, developed a deterministic model for malaria transmission that incorporates a standard incidence rate and treatment. The model assumes that a proportion of individuals who recover or are treated transition to a temporarily immune recovered class, while the remaining individuals revert to the susceptible class. Their numerical simulations support the analytical findings, and the model was applied to real epidemiological data from China covering the period 2003–2013, computing $R_0 = 0.0161$ [8]. S. Kim, et al, [9] studied and analyzed an SIR-SI malaria transmission model incorporating vector-bias to assess its impact on disease dynamics. Their findings indicate that accounting for vector-bias in different regions enhances the ability to predict the future dynamics of malaria and supports informed decision-making in the development of effective control strategies. Liming Cai, et al. [10] proposed a mathematical model for malaria transmission that includes an asymptomatic compartment in the human population and exposed compartments in both humans and mosquitoes. They conducted a stability analysis of the model and found, through simulations, that the overall spread of the disease is higher when all infected individuals exhibit symptoms. Supriatna, Asep K., et al, 2022, an SIR-SI mathematical model, formulated as a system of integral equations, is proposed and analyzed to describe the transmission dynamics of dengue fever between humans and mosquitoes. The findings, derived from both analytical investigations and numerical simulations, indicate that the introduction of Wolbachia has significant potential as a biological control strategy for eliminating dengue infections within the human population [11].

A. Studies on Backward Bifurcation

In 2025, Keno et al performed a rigorous cost-effectiveness analysis to determine the most economical control variable. The possibility of backward bifurcation is suggested by numerical simulation, which reveals the coexistence of a stable disease-free equilibrium (DFE) and a stable endemic equilibrium point (EEP) [12]. AO Sharon, et al, 2025, the posterior estimates of the basic reproductive number (R_0) and mosquito–human ratios provided actionable insights for prioritizing bed net distribution and indoor residual spraying in high-risk regions [13]. The stability analysis of Xiaomei Feng, et al, reveals that when $R_0 < 1$, two endemic equilibria may exist, indicating the occurrence of a backward bifurcation. This implies that malaria can persist even if $R_0 < 1$ [8]. The study conducted by Danbaba, Aloko, and A. Ayinde in 2024, focuses on multiple transmissions, where both vertical and horizontal modes are considered

with application to dengue virus. They have presented a model that incorporates vertical transmission within the mosquito population. Threshold quantities for the model are computed, with the mosquito extinction equilibrium being globally asymptotically stable when the basic offspring number N_0 is less than one; also, the disease-free equilibrium is shown to be locally asymptotically stable when the basic reproduction number R_0 is less than one. The model is shown to undergo backward bifurcation, and conditions under which the disease-free equilibrium would be globally asymptotically stable are presented [14]. G. R. Kelatlhegile, et al, [15] formulated and analyzed a mathematical model for the prevention of a disease that spreads both horizontally and vertically within a population of varying sizes. They conducted a stability analysis of the model and found that multiple endemic equilibria may exist when $R_0 < 1$, indicating the possibility of a backward bifurcation. Their numerical simulations supported and validated the analytical results.

B. Applications of Optimal Control

The study conducted by Adepoju, Okunloye A., and Samson Olaniyi in 2021, investigated a nonlinear model that incorporates vertical transmission and saturated incidence terms. It was further extended to examine the impact of implementing a time-dependent optimal control strategy aimed at blocking the vertical transmission pathway, utilizing Pontryagin's Maximum Principle from optimal control theory. The analytical findings were supported by numerical simulations, which demonstrated that the incorporation of optimal control effectively reduces vertical transmission of the infection and consequently helps to curb the overall spread of the disease within the population [16]. Liming Cai, et al. [10] further applied optimal control theory to their model, incorporating bed nets and treatment as key interventions aimed at reducing both symptomatic and asymptomatic infections. Their simulation results indicate that the implementation of optimal control strategies consistently reduces the number of symptomatic infectious individuals, although it may lead to an increase in the number of asymptomatic infectious individuals.

C. Research Gap and Objectives

In this article, we formulated a new mathematical model different from [8] and the other aforementioned models of malaria transmission. Specifically, we divided the recovered human population into two distinct groups. The first group acquireed partial immunity after recovery and eventually re-entered the susceptible class. The second group might become reinfected immediately after recovery through contact with infectious mosquitoes, with a transmission probability $\delta < 1$, which was lower than that of susceptible individuals. This distinction was not jointly considered in the models reviewed above, and it constitutes the principal contribution of this study. Furthermore, we applied optimal control theory to our model, using optimal control strategies.

The specific objectives of this study are to:

1. formulate an SIR–SI malaria transmission model that incorporates partial immunity and immediate re-infection in the recovered human population;
2. establish the positivity and boundedness of solutions, derive the basic reproduction number R_0 via the next-generation matrix method, and analyze the local and global stability of the disease-free equilibrium;
3. investigate the existence of endemic equilibria and establish analytically and numerically the occurrence of backward bifurcation;
4. calibrate the model to WHO-reported malaria data for the Democratic Republic of Congo and perform a normalized forward sensitivity analysis of R_0; and
5. formulate and numerically evaluate optimal control strategies—bed-net usage, antimalarial treatment, and insecticide spraying—using Pontryagin's Maximum Principle, individually and in combination.

This article is structured as follows: In Section 2, we present the model formulation. Section 3 is devoted to the stability analysis of the model, including the positivity and boundedness of solutions, the existence of equilibria, the occurrence of backward bifurcation, and the global asymptotic stability of the disease-free equilibrium. Numerical simulations are provided in Section 4. In Section 5, we conduct a sensitivity analysis of the basic reproduction number, R_0. Section 6 investigates the optimal control strategies numerically. Section 7 discusses the findings in relation to prior literature and states the model's limitations. Finally, Section 8 provides the conclusion of the article.

2. MATHEMATICAL MODEL

A. Model Description

The human population in our model is divided into three compartments: susceptible humans $S_h(t)$, infectious humans $I_h(t)$, and recovered humans $R_h(t)$. The mosquito population is categorized into two compartments: susceptible mosquitoes $S_m(t)$ and infectious mosquitoes $I_m(t)$. Let $N_h(t)$ and $N_m(t)$ denote the total human and mosquito populations, respectively, such that $N_h(t) = S_h + I_h + R_h$ and $N_m(t) = S_m + I_m$. We assume that mosquito bites occur randomly and that the recovered human population is divided into two subgroups, as previously described: one group possesses partial immunity and re-enters the susceptible class over time, while the other group, lacking immunity, becomes infectious again upon being bitten by an infectious mosquito. Additionally, we assume that both the human and mosquito populations remain constant over time, and that mosquitoes do not recover once infected.

$$\begin{cases} \frac{dS_h}{dt} = \mu N_h - \frac{a\gamma_h S_h I_m}{N_h} - \mu S_h + \rho R_h, \\ \frac{dI_h}{dt} = \frac{\alpha\gamma_h S_h I_m}{N_h} - (\mu+\alpha) I_h + \frac{a\delta\gamma_h R_h I_m}{N_h}, \\ \frac{dR_h}{dt} = \alpha I_h - \frac{a\delta\gamma_h R_h I_m}{N_h} - (\mu+\rho) R_h, \\ \frac{dS_m}{dt} = \psi N_m - \frac{a\gamma_m S_m I_h}{N_h} - \psi S_m, \\ \frac{dI_m}{dt} = \frac{a\gamma_m S_m I_h}{N_h} - \psi I_m, \end{cases} \tag{2.1}$$

with $S_h(0) > 0,\ I_h(0) \geq 0,\ R_h(0) \geq 0,\ S_m(0) > 0,\ I_m(0) \geq 0.$

3. MODEL ANALYSIS

A. Positivity and boundedness of the solutions

Since the total populations of humans and mosquitoes are constant, that is $\frac{dN_h}{dt} = \frac{dN_m}{dt} = 0$, then in order to simplify model (2.1) we normalize the human and mosquito populations. We denote $s_h = \frac{S_h}{N_h},\ i_h = \frac{I_h}{N_h},\ r_h = \frac{R_h}{N_h},\ s_m = \frac{S_m}{N_h},\ i_m = \frac{I_m}{N_h}$ and define in the positive region as

$$\Sigma = \{ (s_h, i_h, r_h, s_m, i_m) \in R_+^5 : 0 \leq s_h + i_h + r_h = 1;\ 0 \leq s_m + i_m \leq 1\}$$

Sine $s_m + i_m = N_m = 1$, this implies that $s_m = 1 - i_m$, the system (2.1) can be written as

$$\begin{cases} \frac{ds_h}{dt} = \mu - aq\gamma_h s_h i_m - \mu s_h + \rho r_h, \\ \frac{di_h}{dt} = aq\gamma_h s_h i_m - (\mu+\alpha) i_h + aq\delta\gamma_h r_h i_m, \\ \frac{dr_h}{dt} = \alpha i_h - aq\delta\gamma_h r_h i_m - (\mu+\alpha) r_h, \\ \frac{ds_m}{dt} = \psi - a\gamma_m s_m i_h - \psi s_m, \\ \frac{di_m}{dt} = a\gamma_m s_m i_h - \psi i_m, \end{cases} \tag{3.1}$$

Sine $s_m = 1 - i_m$ then we can omit s_m from the model (3.1), and rearrange it as

$$\begin{cases} \frac{ds_h}{dt} = \mu - aq\gamma_h s_h i_m - \mu s_h + \rho r_h, \\ \frac{di_h}{dt} = aq\gamma_h s_h i_m - (\mu+\alpha) i_h + aq\delta\gamma_h r_h i_m, \\ \frac{dr_h}{dt} = \alpha i_h - aq\delta\gamma_h r_h i_m - (\mu+\rho) r_h, \\ \frac{di_m}{dt} = a\gamma_m (1 - i_m) i_h - \psi i_m, \end{cases} \tag{3.2}$$

where the model (3.2) is defined on the feasible region

$$\Upsilon = \{ (s_h, i_h, r_h, i_m) \in R_+^4 : 0 \leq s_h + i_h + r_h = 1,\ 0 \leq i_m \leq 1\},$$

B. Existence of Equilibria

It is evident that the system (3.2) admits a disease-free equilibrium at P_0=(1, 0, 0, 0). To compute the basic reproduction number, we apply the next generation matrix method as described in [18, 19]. R_0 at P_0, let,

$$F = \begin{bmatrix} aq\gamma_h s_h i_m + a\delta\gamma_h r_h i_m \\ 0 \\ a\gamma_m (1 - i_m) i_h \end{bmatrix}, V = \begin{bmatrix} (\mu+\alpha) i_h \\ \alpha i_h - aq\delta\gamma_h r_h i_m - (\mu+\alpha) r_h \\ \psi i_m \end{bmatrix}$$

Differentiate F and V partially with respect to: i_h, r_h, i_m at P_0(1, 0, 0, 0), we obtain:

$$f = \begin{bmatrix} 0 & 0 & aq\gamma_h \\ 0 & 0 & 0 \\ a\gamma_m & 0 & 0 \end{bmatrix} and\ v = \begin{bmatrix} (\mu+\alpha) & 0 & 0 \\ -\alpha & (\mu+\rho) & 0 \\ 0 & 0 & \psi \end{bmatrix}$$

$$fv^{-1} = \begin{bmatrix} 0 & 0 & aq\gamma_h \\ 0 & 0 & 0 \\ a\gamma_m & 0 & 0 \end{bmatrix} \begin{bmatrix} \frac{1}{(\mu+\alpha)} & 0 & 0 \\ \frac{\alpha}{(\mu+\alpha)(\mu+\rho)} & \frac{1}{(\mu+\alpha)} & 0 \\ 0 & 0 & \frac{1}{\psi} \end{bmatrix} = \begin{bmatrix} 0 & 0 & \frac{aq\gamma_h}{\psi} \\ 0 & 0 & 0 \\ \frac{a\gamma_m}{(\mu+\alpha)} & 0 & 0 \end{bmatrix}$$

The reproduction number R_0 is given by the spectral radius of fv^{-1} which is denoted by σfv^{-1} and defined as

$$R_0 = \sigma fv^{-1} = \sqrt{\frac{a^2 q\gamma_h\gamma_m}{\psi(\mu+\alpha)}} \qquad (3.3)$$

where σ is the spectral radius of the next generation matrix fv^{-1}.

Local stability of disease-free equilibrium

In this subsection, we investigate the stability of the disease-free equilibrium P_0 by analyzing the model (3.2). This is done by computing the Jacobian matrix evaluated at the equilibrium point P_0, and the resulting expression is obtained as follows

$$J(P_0) = \begin{bmatrix} -\mu & 0 & \rho & -aq\gamma_h \\ 0 & -(\mu+\alpha) & 0 & aq\gamma_h \\ 0 & \alpha & -(\mu+\rho) & 0 \\ 0 & a\gamma_m & 0 & -\psi \end{bmatrix}$$

To find the eigenvalues of the above matrix we use determinant

$$|J(P_0) - \lambda I| = \begin{vmatrix} -\mu-\lambda & 0 & \rho & -aq\gamma_h \\ 0 & -(\mu+\alpha)-\lambda & 0 & aq\gamma_h \\ 0 & \alpha & -(\mu+\rho)-\lambda & 0 \\ 0 & a\gamma_m & 0 & -\psi-\lambda \end{vmatrix} = 0$$

The two eigenvalues of the above jacobian matrix are clearly negative, (i.e $\lambda_1 = -\mu\ and\ \lambda_2 - (\mu + \rho)$). The other two roots can be characterized as:

$$\lambda^2 + b_1\lambda + b_2 = 0 \qquad (3.4)$$

where $b_1 = \mu + \alpha,\ b_2 = \psi(\mu+\alpha)(1 - R_0^2)\ and\ \mu, \alpha > 0, so\ b_1 > 0$

Using the Routh-Hurwitz Criterion [20] the two eigenvalues of the characteristic equation (3.4) have negative real part if and only if

$$b_1 > 0\ ,\ \ b_1 b_2 > 0 \qquad (3.5)$$

if $R_0 < 1$, then $b_2 > 0$, Hence $b_1 b_2 > 0$. Thus, we have the following theorem.

Theorem 3.1. The disease-free equilibrium P_0 of model (3.2) is locally asymptotically stable if and only if $R_0 < 1$ and the inequalities (3.5) are satisfied.

Endemic Equilibrium and Bifurcation

To determine the endemic equilibrium of system (3.2), we set $\frac{dS_h}{dt} = \frac{dI_h}{dt} = \frac{dR_h}{dt} = \frac{dI_m}{dt} = 0$. After straightforward calculations, we obtain the endemic equilibrium point $P^* = (S_h^*, I_h^*, R_h^*, I_m^*)$ for the model (3.2) as follows:

$$\left.\begin{aligned} s_h^* &= \frac{a\mu\gamma_m(1-i_m^*)\big((\mu+\rho)+aq\delta\gamma_h i_m^*\big) + \rho\alpha\psi i_m^*}{(aq\gamma_h i_m^*)\big(\alpha\gamma_m(1-i_m^*)(\mu+\rho+aq\delta\gamma_h i_m^*)\big)} \\ i_h^* &= \frac{\psi i_m^*}{\alpha\gamma_m(1-i_m^*)}, r_h^* = \frac{\alpha\psi i_m^*}{\alpha\gamma_m(1-i_m^*)\big((\mu+\rho)+aq\delta\gamma_h i_m^*\big)} \end{aligned}\right\} \qquad (3.6)$$

Next, we substitute equation (3.6) into the second equation of system (3.2) to obtain a quadratic equation, which is given by:

$$g(i_m^*) = c_1 {i_m^*}^2 + c_2 i_m^* + c_3 = 0, \quad (3.7)$$

$c_1 = a^2 q^2 \delta {\gamma_h}^2 \psi \mu$

$c_2 = aq\delta\mu^2\psi\gamma_h + aq\psi\gamma_h\mu(\mu+\rho+\alpha) + aq\mu\gamma_h\gamma_m + \left(a(\mu+\rho) + q\gamma_h(\delta+a)\right)$

$c_3 = (\mu+\alpha)(\mu+\rho)\psi\mu(1-R_0^2),$

Consequently, from equations (3.7),(3.8), and the parameter values provided in Table 1 below, it is evident that the possibility of multiple endemic equilibria exists. This implies that the phenomenon of backward bifurcation may occur. As a result, we state the following theorem.

Table 1: Number of possible real roots of equation (3.7)

Case	c_1	c_2	c_3	R_0	No. of sign changes	No. of possible real roots
1	+	+	+	$R_0<1$	0	0
2	+	+	–	$R_0>1$	1	1
3	+	–	+	$R_0<1$	2	0, 2
4	+	–	–	$R_0>1$	1	1

Theorem 3.2. The system (3.2) has a unique endemic equilibrium p^*, if $R_0 > 1$ and When cases 2,4 are satisfied and the system (3.2) could have more than one endemic equilibrium if $R_0 < 1$ and case 3 are satisfied. That is the following conditions are true for model (3.2)

(i) if $c_3 < 0$, $R_0 > 1$, exactly the system (3.2) has one endemic equilibrium.

(ii) exactly one unique endemic equilibrium if $c_2 < 0$ and $c_3 = 0$ *or* $c_2^2 - 4c_2c_3 = 0$.

(iii) exactly two endemic equilibriums if $c_3 > 0$, (i.e. $R_0 < 1$), $c_2 < 0$, and $c_2^2 - 4c_1c_3 > 0$.

(iv) no endemic equilibrium otherwise.

The system (3.1) can be written in the form $x'(t) = f(x)$, where $x = (x_1, x_2, x_3, x_4, x_5) = (s_h, i_h, r_h, s_m, i_m)$ and $f = (f_1(x), f_2(x), f_3(x), f_4(x), f_5(x))$, denotes the R.H.S. of the system (3.2) as:

$$\begin{cases} \frac{dx_1}{dt} = \mu - aq\gamma_h x_1 x_5 - \mu x_1 + \rho x_3, \\ \frac{dx_2}{dt} = aq\gamma_h x_1 x_5 - (\mu+\alpha)x_2 + aq\delta\gamma_h x_3 x_5, \\ \frac{dx_3}{dt} = \alpha i_h - aq\delta\gamma_h x_3 x_5 - (\mu+\alpha)x_3, \\ \frac{dx_4}{dt} = \psi - a\gamma_m x_2 x_4 - \psi x_4, \\ \frac{dx_5}{dt} = a\gamma_m x_2 x_4 - \psi x_5, \end{cases} \quad (3.8)$$

(3.9)

we evaluate the Jacobian matrix of the system (3.8) at P_0, which is denoted by $J(P_0)$. And it is given by

$$J(P_0) = \begin{bmatrix} -\mu & 0 & \rho & 0 & -aq\gamma_h \\ 0 & -(\mu+\alpha) & 0 & 0 & aq\gamma_h \\ 0 & \alpha & -(\mu+\rho) & 0 & 0 \\ 0 & -a\gamma_m & 0 & -\psi & 0 \\ 0 & a\gamma_m & 0 & 0 & -\psi \end{bmatrix} = 0$$

Next, we consider $R_0 = 1$. Furthermore, let $\gamma_h = \gamma^*$chosen to be the bifurcation parameter. Solving equation (3.3) for γ_h with $R_0 = 1$ yields

$$\gamma_h = \gamma^* = \frac{(\mu+\alpha)\psi}{a^2 q \gamma_m},$$

After simple calculation it is easy to see that $J(P_0)$ with $\gamma_h = \gamma^*$, denoted by J_{γ^*}, has a simple zero eigenvalue and other eigenvalues have negative real part. i.e $\left(\lambda_1 = 0,\ \lambda_2 = -\mu,\ \lambda_3 = -(\mu+\rho),\ \lambda_4 = -\frac{1}{2}(\alpha + 2\mu) - \frac{1}{2}\sqrt{a^2 - 4aq\gamma_h\gamma_m},\ \lambda_4 = -\frac{1}{2}(\alpha+2\mu) + \frac{1}{2}\sqrt{a^2 - 4aq\gamma_h\gamma_m},\right)$. Hence, the dynamics of the system (3.8) satisfy the conditions of the center manifold theory [21]. Moreover, we show that the system (3.8) is equivalent to system (3.2), underdoes backward bifurcation at $R_0 = 1$, then we apply the Centre Manifold Theorem to test the dynamics of (3.2) close to $\gamma_h = \gamma^*$.

The Jacobian matrix of the system (3.2), denoted by $J(P_0)$ at $\gamma_h = \gamma^*$, has a right and a left eigenvectors associated with zero eigenvalue, given by: $w = (w_1, w_2, w_3, w_4, w_5)^T$, and $(v_1, v_2, v_3, v_4, v_5)$ respectively. Where

$$\left.\begin{aligned} w_1 &= \frac{-aq\gamma^*(\mu+\alpha+\rho)w_5}{(\mu+\alpha)(\mu+\rho)}, w_2 = \frac{aq\gamma^* w_5}{(\mu+\alpha)}, \\ w_3 &= \frac{-a\alpha q\gamma^* w_5}{(\mu+\alpha)(\mu+\rho)}, w_4 = \frac{-a^2 q\gamma_m\gamma^* w_5}{\psi(\psi+\alpha)}, w_5 = w_5 \end{aligned}\right\}$$

$$and\ v_1 = 0, v_2 = v_2, v_3 = 0, v_4 = 0, v_5 = \frac{aq\gamma^* v_2}{\psi} \quad (3.11)$$

To show the existence of backward bifurcation, we compute $\frac{\partial^2 f_i}{\partial x_i \partial x_j}$, where $i, j = 1, 2, 3, 4, 5$. at P_0 and obtain

$$\left.\begin{aligned} &\frac{\partial^2 f_2}{\partial x_1 \partial x_5} = \frac{\partial^2 f_2}{\partial x_5 \partial x_1} = aq\gamma_h, \quad \frac{\partial^2 f_2}{\partial x_3 \partial x_5} = \frac{\partial^2 f_2}{\partial x_5 \partial x_3} = aq\delta\gamma_h, \\ &\frac{\partial^2 f_2}{\partial x_2 \partial x_4} = \frac{\partial^2 f_2}{\partial x_4 \partial x_2} = a\gamma_m, \quad \frac{\partial^2 f_5}{\partial x_2 \partial x_4} = \frac{\partial^2 f_2}{\partial x_4 \partial x_2} = a\gamma_h \end{aligned}\right\} \quad (3.12)$$

Now we compute the factors a and b defined in Theorem 4.1 [21] of Castillo-Chavez and Song as follows

$$\left.\begin{aligned} a &= \sum_{k,i,j=1}^{n} v_k w_i w_j \frac{\partial^2 f_k}{\partial x_i \partial x_j}(0, \gamma^*) \\ &= \sum_{i,j=1}^{n} v_2 w_i w_j \frac{\partial^2 f_2}{\partial x_i \partial x_j}(0, \gamma^*) + \sum_{i,j=1}^{n} v_5 w_i w_j \frac{\partial^2 f_5}{\partial x_i \partial x_j}(0, \gamma^*) \\ a &= \sum_{i,j=1}^{n} 2v_2 w_1 w_5 \frac{\partial^2 f_2}{\partial x_1 \partial x_5}(0, \gamma^*) \\ &\quad + \sum_{i,j=1}^{n} 2v_2 w_3 w_5 \frac{\partial^2 f_2}{\partial x_3 \partial x_5}(0, \gamma^*) + \sum_{i,j=1}^{n} 2v_5 w_2 w_4 \frac{\partial^2 f_5}{\partial x_2 \partial x_5}(0, \gamma^*) \\ &= 2aq\gamma_h v_2 w_1 w_5 + 2aq\delta\gamma_h v_2 w_3 w_5 + 2a\gamma_m v_5 w_2 w_4, \end{aligned}\right\} \quad (3.13)$$

and

$$\left.\begin{aligned} b &= \sum_{k,i,j=1}^{n} v_k w_i w_j \frac{\partial^2 f_k}{\partial x_i \partial \gamma}(0, \gamma^*) \\ &= \sum_{i=1}^{n} v_2 w_i \frac{\partial^2 f_2}{\partial x_i \partial \gamma}(0, \gamma^*) = a^2 q^2 \gamma^* v_2^2 > 0 \end{aligned}\right\} \quad (3.14)$$

Since the factor b is always positive, then model (3.1) undergoes backward bifurcation at $R_0 = 1$, whenever

$$a = 2aq\gamma_h v_2 w_1 w_5 + 2aq\delta\gamma_h v_2 w_3 w_5 + 2a\gamma_m v_5 w_2 w_4 > 0. \quad (3.15)$$

Then we can establish from the above discussions the following theorem.

Theorem 3.3. The system (3.1) undergoes a backward bifurcation at R_0 whenever inequality (3.15) holds.

Local stability of endemic equilibrium

Theorem 3.4. For $R_0 > 1$, the endemic equilibrium P^* of system (3.1) is locally asymptotically stable if condition (3.18) is satisfied; otherwise, it is unstable.

Proof. At P^*, the Jacobian matrix $J(P^*)$ is evaluated as

$$J(P_0) = \begin{bmatrix} -\mu - z_1 & 0 & \rho & -z_2 \\ z_1 & -z_3 & z_4 & z_5 \\ 0 & \alpha & -z_6 & -z_5 \\ 0 & z_7 & 0 & -z_8 - \psi \end{bmatrix}, \quad (3.16)$$

where $z_1 = aq\gamma_h i_m^*,\ z_2 = aq\gamma_h s_h^*,\ z_3 = (\mu+\alpha),\ z_4 = aq\delta\gamma_h r_h^*,\ z_5 = aq\delta\gamma_h i_m^*,\ z_6 = (\mu+\rho),\ z_7 = a\gamma_m(1 - i_m^*),\ z_8 = a\gamma_m i_h^*$

The roots of the matrix (3.16) can be determined from the following characteristics equation

$$f(\lambda) = \lambda^4 + a_1\lambda^3 + a_2\lambda^2 + a_3\lambda + a_4 = 0, \quad (3.17)$$

where $a_1 = z_1 + z_1 + z_1 + z_1 + \mu + \psi$

$$a_2 = (z_1 + \mu)(z_3 + z_6 + z_8 + \psi) + (z_3 + z_6)(z_8 + \psi) + z_1 z_6 - (\alpha z_4 + z_5 z_7),$$

$$a_3 = (z_1 + \mu)\big(z_3 z_6 + z_3(z_8 + \psi)\big) + z_6(z_8 + \psi) - (\alpha z_4 + z_5 z_7) + (z_3 z_6 - \alpha z_4)(z_8 + \psi) + z_5 z_7(z_4 - z_6) + z_7 - \alpha\rho z_1$$

$$a_4 = (z_1 + \mu)(z_3 z_6 - \alpha z_4) + z_7(z_4 z_5 - z_5 z_6)(z_1 + \mu)\rho z_1 + z_1 z_2 + z_6 z_7.$$

The Rouuth-Hurtwiz criteria [22] for equation (3.17) will give four negative eigenvalues if and only if $c_i > 0$, for i = 1, 2, 3, 4 and the following condition is satisfied

$$a_1 a_2 a_3 > a_3^2 + a_1^2 a_4 \quad (3.18)$$

Thus, the system (3.2) about P^* is locally asymptotically stable if $R_0 > 1$ and the condition (3.18) is satisfied.

Global Asymptotic Stability of Disease-Free Equilibrium

Theorem 3.5. The disease-free equilibrium p_0 of model (3.1) is globally asymptotically stable if $R_0 < 1$ and satisfies $\delta < 1$.

Proof. To prove the global stability of p_0 we define the Lyapunov function as

$$V = a\gamma_m i_h + (\mu + \alpha) i_m,$$

$$V' = a\gamma_m i'_h + (\mu + \alpha) i'_m,$$

$$= a\gamma_m [aq\gamma_h s_h i_m - (\mu + \alpha) i_h + aq\delta\gamma_h r_h i_m] + (\mu + \alpha)[a\gamma_m s_m i_h - \psi i_m]$$

$$\leq a\gamma_m aq\gamma_h (s_h + r_h) i_m - \psi(\mu + \alpha) i_m - (\mu + \alpha)\gamma_m i_m i_h$$

$$\leq \psi(\mu + \alpha)\left[\frac{a\gamma_m aq\gamma_h (s_h + r_h)}{\psi(\mu + \alpha)} - 1\right] i_m - (\mu + \alpha)\gamma_m i_m i_h$$

$$\leq \psi(\mu + \alpha) i_m [R_0^2 (s_h + i_h) - 1] - (\mu + \alpha)\gamma_m i_m i_h$$

$$\leq \psi(\mu + \alpha) i_m [R_0^2 - 1] - (\mu + \alpha)\gamma_m i_m i_h$$

$$\leq \psi(\mu + \alpha) i_m [R_0^2 - 1].$$

Then from $R_0 < 1$ and $\delta < 1$, we have $V' = 0$ if and only if $i_m = 0$. And from the second equation of (3.1), we have $\lim_{t\to\infty} i_h(t) = 0$ also from the first and third equations of (3.1) we have $\lim_{t\to\infty} r_h(t) = 0$, $\lim_{t\to\infty} s_h(t) = 1$ and $\lim_{t\to\infty} s_m(t) = 1$ respectively. Furthermore, the largest compact invariant set in $(s_h, i_h, r_h, s_m, i_m) \in \Upsilon : V' = 0$ is the singleton P_0, where P_0 is the disease-free equilibrium point. Using LaSalle's invariant principle, it implies that P_0 is globally asymptotically stable in Υ if $R_0<1$ and $\delta < 1$. Hence proved.

4. NUMERICAL SIMULATIONS

We applied our model to simulate the reported malaria data from the Democratic Republic of the Congo (DRC) [23, 24].

Data processing: The cumulative malaria case counts used for model fitting were extracted from the WHO Global Health Observatory and successive World Malaria Reports for the years 2011–2022 [23, 24]. Because these two sources do not report on identical schedules, the annual series were cross-checked for consistency, and years with ambiguous or revised figures (notably 2017 and 2020, where reporting was affected by surveillance disruptions) were retained but flagged as lower-confidence points during fitting. No interpolation of missing years was required, as a complete annual series was available; however, the cumulative series is smoothed by construction, which limits the sensitivity of the nonlinear least-squares fit to short-term reporting noise but should be kept in mind when interpreting year-to-year deviations in Figure 2.

Table 2: Description of parameters of the model

Parameter	Parameter description	Value	Reference
a	Mosquito biting rate	0.3*356	[25]
ψ	Natural death rate of mosquitoes	24.333	[25]
μ	Natural death rate of humans	0.01538	[26]
ρ	Loss of immunity rate for humans	1.0357	Fitting
α	Recovery rate of humans	2.9670	Fitting
γ_h	Transmission rate in humans	0.01	[27]
γ_m	Transmission rate in mosquitoes	0.3	[27]
δ	Transmission probability of recovered humans	0.043	Fitting

Figure (1) presents the temporal evolution of the cumulative number of reported malaria cases of the DRC over the period from 2011 to 2022. The horizontal axis represents the calendar year, while the vertical axis quantifies the cumulative number of malaria cases. A blue solid line connects the cumulative data values across years, representing the trend in malaria burden over time, and red star markers indicate the individual yearly data points, which are explicitly labeled as (Data Points) in the plot legend. From 2011 to 2014, the data show a monotonic increase in cumulative cases, indicating sustained transmission and possible under performance of control interventions, and in 2014 and 2016, the curve exhibited a plateau, suggesting a period of near-

stabilization in the cumulative count-possibly due to enhanced control measures, changes in surveillance, or underreporting. A marked resurgence has been observed beginning in 2017, with a significant increase through 2019. In 2020, the cumulative curve shows a slight deceleration or stagnation, which may reflect disruptions in health services or reporting inconsistencies. The cumulative count resumes a sharp upward trajectory in 2021 and 2022, ultimately approaching 30 million cases by the end of the observed period.

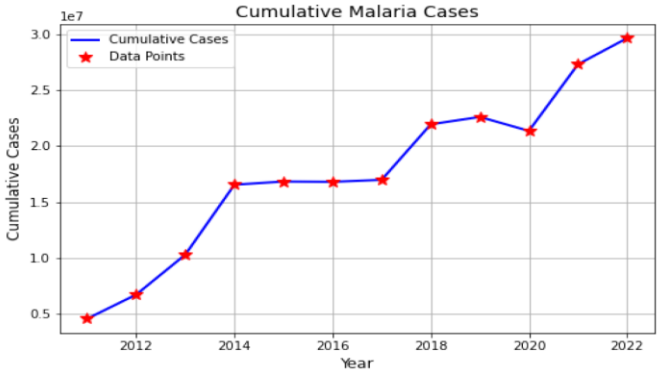


Figure 1: Cumulative malaria reported cases for DRC from WHO [23, 24].

Figure (2) presents a comparison between observed cumulative malaria cases and a fitted model (2.1) over the period 2011–2022. The blue dots indicate the empirical data extracted from WHO reports [23, 24], representing the observed cumulative malaria cases for each year and the orange curve corresponds to a nonlinear fitted of model (2.1), which aims to approximate the temporal trend of the observed data. The model (2.1) fit is quantified by the coefficient of determination, $R^2 = 0.836$, which is annotated at the top of the plot. The fitted curve captures the general trajectory of the data, particularly during the earlier and mid-years (2011–2017), where model predictions align closely with observed points. Some discrepancies are noted in the later years (2018–2022), where the observed data fluctuated more sharply, deviating above or below the model curve. The reported R^2 value of 0.836 indicates a reasonably strong fit, implying that approximately 83.6% of the variance in the cumulative malaria data is explained by our model.

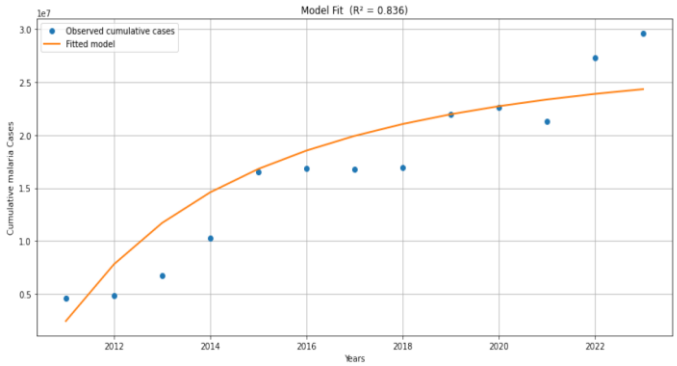


Figure 2: Comparison between observed cumulative malaria cases and a fitted model from 2011 to 2022 for DRC [23, 24].

Figure (3) presents the empirical distributions of two model parameters, ρ (left) and α (right), obtained through bootstrap resampling. Bootstrap analysis is a non-parametric statistical method used to assess the uncertainty in parameter estimates by generating multiple resampled datasets and refitting the model to each. The x-axis denotes the resampled estimates of the parameter ρ and the y-axis represents the frequency of these estimates across bootstrap iterations. The distribution is right-skewed, with a long tail extending toward higher values and a sharp peak at the upper bound (around 3), suggesting that the optimization may be constrained or that ρ is sensitive to the dataset. A vertical red dashed line indicates the original fitted value of ρ, which appears to be approximately 1.0, close to the mode of the distribution. The wide spread of the distribution and clustering near the bounds may imply high variability or identifiability issues (the right panel of Figure (3) histogram of α). The x-axis displays the bootstrap estimates of the parameter α. The distribution is approximately symmetric and bell-shaped, centered around the fitted value of 2.98, which is again marked by the vertical red dashed line. The spread is relatively narrow, indicating that the parameter estimate is stable and well-identified under resampling. This suggests a higher confidence in the estimate of α compared to ρ. The bootstrap distribution of ρ reveals substantial variability, suggesting that this parameter is less robust and may be sensitive to data fluctuations or boundaries imposed during model fitting. In contrast, α shows a tight concentration around its fitted value, supporting the strong reliability of its estimate. These distributions are critical for constructing confidence intervals, quantifying

parameter uncertainty, and performing sensitivity analysis in model-based inference.

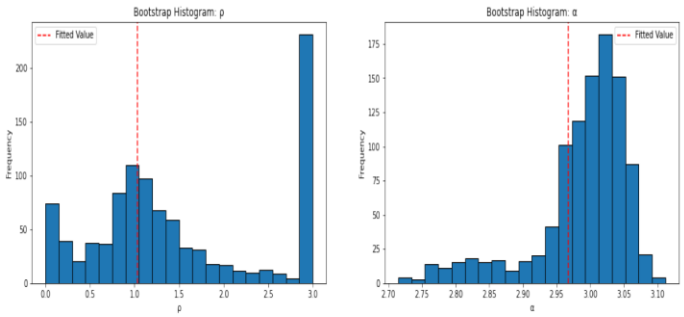


Figure 3: Bootstrap Distributions of Parameters ρ and α

5. SENSITIVITY ANALYSIS

A sensitivity analysis was performed to evaluate the influence of model parameters on the dynamics of malaria transmission. This analysis offers valuable insights into the parameters that exert the greatest impact on the theoretical behavior of the model, with particular emphasis on the basic reproduction number, R_0. The normalized forward sensitivity index was employed to quantify these effects, as it measures the relative change in a model output in response to a relative change in a given parameter. Figure (4) illustrates the relationship between the basic reproduction number R_0 and transmission rate in humans γ_h, providing insight into the bifurcation behavior of the system (2.1) under study. The X-axis represents the transmission rate in humans, γ_h, varying from 0 to 1 and the Y-axis represents the basic reproduction number R_0, a threshold quantity indicating the average number of secondary infections generated by a single infectious individual in a fully susceptible population. The blue curve shows the variation of R_0 as a function of γ_h. It is monotonically decreasing as γ_h increases, R_0 decreases. The red dashed line indicates the epidemiological threshold, $R_0 = 1$, separating disease eradication ($R_0 < 1$) from persistence ($R_0 > 1$). Magenta Circle marks the bifurcation point, i.e., the critical value of γ_h at which $R_0 = 1$. This is the epidemic threshold where trans-critical bifurcation typically occurs. The disease-free equilibrium changes stability as R_0 crosses 1. The figure provides essential insights for control strategies specifically, improving recovery (e.g., through treatment) can drive the system below the epidemic threshold.

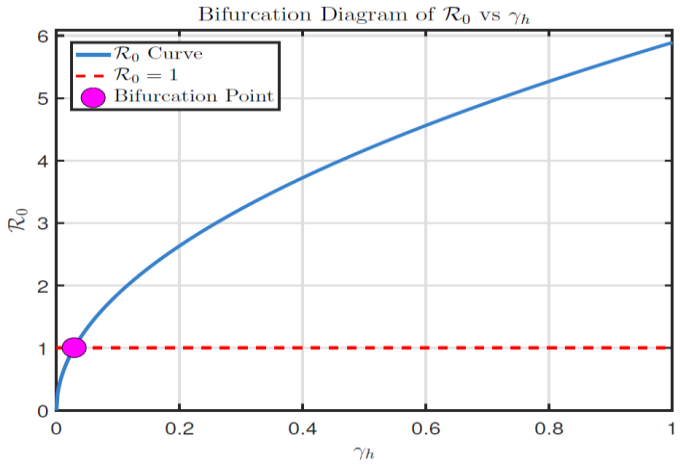


Figure 4: Bifurcation diagram of R_0 vs. γ_h

6. OPTIMAL CONTROL

In this section, we apply Pontryagin's Maximum Principle to derive the necessary conditions for the existence of an optimal control strategy for the malaria transmission model. Time-dependent control variables are incorporated into the model to identify effective intervention strategies aimed at mitigating malaria transmission. We consider three control variables: $u_1(t)$, $u_2(t)$, and $u_3(t)$, which represent the following intervention efforts: $u_1(t)$, effort to prevent malaria infections using bed nets. $u_2(t)$, treatment control through the distribution of antimalarial drugs to infected individuals, and $u_3(t)$, spraying of insecticides to reduce mosquito populations. The objective is to determine an optimal control strategy that minimizes the number of infected individuals and the associated costs of implementing the control measures. The structure of the objective functional is analogous to that used in standard optimal control problems governed by [15, 28] and it's given by:

$$J(u_1, u_2, u_3) = \int_0^{t_f} (AI_h + c_1u_1^2 + c_2u_2^2 + c_3u_3^2)\, dt, \qquad (6.1)$$

where A is the balancing cost factor used to normalize the objective functional, and c_1, c_2, and c_3 are the weighting constants associated with the use of bed nets, treatment of infected individuals, and insecticide spraying, respectively. These weights reflect the relative cost or importance of each control measure in reducing the spread of malaria. Consequently, we seek to determine the optimal control functions $u_1^*(t), u_2^*(t)\ and\ u_3^*(t)$ such that they minimize the objective functional subject to the dynamics of the controlled malaria transmission model and the associated constraints.

$$\left.\begin{array}{l} J(u_1^*, u_2^*, u_3^*) = min\, J(u_1, u_2, u_3), \\ \Gamma = \{(u_1, u_2, u_3) |\ 0 \le u_i \le 1, i = 1,2,3\} \end{array}\right\} \qquad (6.2)$$

$$\begin{cases} \frac{dS_h}{dt} = \mu N_h - a(1-u_1)\frac{\gamma_h S_h I_m}{N_h} - \mu S_h + \rho R_h, \\ \frac{dI_h}{dt} = a(1-u_1)\frac{\gamma_h S_h I_m}{N_h} - (\mu + u_2\alpha)I_h + \frac{a\delta\gamma_h R_h I_m}{N_h}, \\ \frac{dR_h}{dt} = u_2\alpha I_h - \frac{a\delta\gamma_h R_h I_m}{N_h} - (\mu+\rho)R_h, \\ \frac{dS_m}{dt} = \psi N_m(1-u_3) - a(1-u_1)\frac{\gamma_m S_m I_h}{N_h} - (u_3+\psi)S_m, \\ \frac{dI_m}{dt} = a(1-u_1)\frac{\gamma_m S_m I_h}{N_h} - (u_3+\psi)I_m, \end{cases} \quad (6.3)$$

The optimal control must satisfy the necessary conditions derived from Pontryagin's Maximum Principle [29]. This principle transforms the system of equations (6.2) and (6.3) into an optimal control problem characterized by the pointwise minimization of a Hamiltonian function *H* with respect to the control variables u_1, u_2, and u_3.

$$\begin{aligned} H = {} & AI_h + c_1u_1^2 + c_2u_2^2 + c_3u_3^2 \\ & + \lambda_{S_h}\left[\mu N_h - a(1-u_1)\frac{\gamma_h S_h I_m}{N_h} - \mu S_h + \rho R_h\right] \\ & + \lambda_{I_h}\left[a(1-u_1)\frac{\gamma_h S_h I_m}{N_h} - (\mu+u_2\alpha)I_h + \frac{a\delta\gamma_h R_h I_m}{N_h}\right] \\ & + \lambda_{R_h}\left[u_2\alpha I_h - \frac{a\delta\gamma_h R_h I_m}{N_h} - (\mu+\rho)R_h\right] \\ & + \lambda_{S_m}\left[\psi N_m(1-u_3) - a(1-u_1)\frac{\gamma_m S_m I_h}{N_h} - (u_3+\psi)S_m\right] \\ & + \lambda_{I_m}\left[a(1-u_1)\frac{\gamma_m S_m I_h}{N_h} - (u_3+\psi)I_m\right] \end{aligned} \quad (6.4)$$

where $\lambda_{S_h}, \lambda_{I_h}, \lambda_{R_h}, \lambda_{S_m}, \lambda_{I_m}$ represents the adjoint variables. The solution to the system is obtained by appropriately taking the partial derivatives of the Hamiltonian (6.4) with respect to the corresponding state variables.

Theorem 6.1. Given optimal controls $u_1^*, u_2^* \text{ and } u_3^*$ and solutions S_h, I_h,R_h, S_m, I_m of the co-responding state System (6.3) and (6.4) that minimize $J(u_1)$ over Γ. Then there exists adjoint variables $\lambda_{S_h}, \lambda_{I_h}, \lambda_{R_h}, \lambda_{S_m}, \lambda_{I_m}$ satisfying

$$\frac{d\lambda_i}{dt} = -\frac{\partial H}{\partial i}, \quad (6.5)$$

where i = S_h, I_h, R_h, S_m, I_m, with transversality conditions

$$\lambda_{S_h}(t_f) = \lambda_{I_h}(t_f) = \lambda_{R_h}(t_f) = \lambda_{S_m}(t_f) = \lambda_{I_m}(t_f) = 0, \quad (6.6)$$

$$u_1^* = min\left\{1, max\left\{0, \frac{a}{2c_1N_h}\left[\gamma_h S_h I_m(\lambda_{S_h} - \lambda_{I_h}) + \gamma_m S_m I_h(\lambda_{I_m} - \lambda_{S_m})\right]\right\}\right\} \quad (6.7)$$

$$u_2^* = min\left\{1, max\left\{0, \frac{\alpha I_h}{2c_2}(\lambda_{I_h} - \lambda_{R_h})\right\}\right\} \quad (6.8)$$

$$u_3^* = min\left\{1, max\left\{0, \frac{1}{2c_3}\left[(\psi N_m + S_m)\lambda_{S_m} + I_m\lambda_{I_m}\right]\right\}\right\} \quad (6.9)$$

Proof: Theorem 4.1 and Corollary 4.1 of [29] provide sufficient conditions for the existence of an optimal control, based on the convexity of the integrand of the objective functional J(u_1, u_2, u_3) with respect to the control variables u_1, u_2 and u_3, the a priori boundedness of the state solutions, and the Lipschitz continuity of the state system with respect to the state variables. The Hamiltonian function, evaluated at the optimal control level, gives rise to the corresponding adjoint variables. Consequently, the adjoint equations can be expressed as follows:

$$\begin{aligned} \frac{d\lambda_{S_h}}{dt} = {} & a(1-u_1)\frac{\gamma_h I_m}{N_h}(\lambda_{S_h} - \lambda_{I_h})a(1-u_1)\frac{\gamma_h S_h I_m}{N_h^2}(\lambda_{I_h} - \lambda_{S_h}) \\ & + \frac{a\delta\gamma_h R_h I_m}{N_h^2}(\lambda_{I_h} - \lambda_{R_h}) + a(1-u_1)\frac{\gamma_m S_m I_h}{N_h^2}(\lambda_{I_m} - \lambda_{S_m}) + \mu\lambda_{S_h}, \\ \frac{d\lambda_{I_h}}{dt} = {} & -A + a(1-u_1)\frac{\gamma_h S_h I_m}{N_h^2}(\lambda_{I_h} - \lambda_{S_h}) + \frac{a\delta\gamma_h R_h I_m}{N_h^2}(\lambda_{I_h} - \lambda_{R_h}) \\ & + a(1-u_1)\frac{\gamma_m S_m I_h}{N_h^2}(\lambda_{I_m} - \lambda_{S_m}) + a(1-u_1)\frac{\gamma_m S_m}{N_h^2}(\lambda_{S_m} - \lambda_{I_m}) \\ & + (\mu + u_2\alpha)\lambda_{I_h} + u_2\alpha\lambda_{R_h}, \\ \frac{d\lambda_{R_h}}{dt} = {} & a(1-u_1)\frac{\gamma_h S_h I_m}{N_h^2}(\lambda_{I_h} - \lambda_{S_h}) + \frac{a\delta\gamma_h I_m}{N_h}(\lambda_{R_h} - \lambda_{I_h}) \\ & + a(1-u_1)\frac{\gamma_m S_m I_h}{N_h^2}(\lambda_{I_m} - \lambda_{S_m}) + \frac{a\delta\gamma_h R_h I_m}{N_h^2}(\lambda_{I_h} - \lambda_{R_h}) + (\mu\rho)\lambda_{R_h} - \rho\lambda_{S_h}, \\ \frac{d\lambda_{S_m}}{dt} = {} & a(1-u_1)\frac{\gamma_m I_h}{N_h}(\lambda_{S_m} - \lambda_{I_m}) + (u_3+\psi)\lambda_{S_m}, \\ \frac{d\lambda_{I_m}}{dt} = {} & a(1-u_1)\frac{\gamma_h S_h}{N_h}(\lambda_{S_h} - \lambda_{I_h}) + \frac{a\delta\gamma_h R_h}{N_h}(\lambda_{R_h} - \lambda_{I_h}) + (u_3+\psi)\lambda_{I_m} \end{aligned} \quad (6.10)$$

A. Numerical Simulations for Optimal Control

In this subsection, we employ a MATLAB program to obtain the numerical solutions of the model. The parameter values used for these simulations are presented in Table 3.

Prevention of malaria using bed-net (u_1(t)) only

The analysis of Figure (5) evaluates the impact of implementing a single control measure, u_1(t), while keeping the other controls, u_2(t) and u_3(t), inactive. The results indicate that applying only u_1(t) substantially reduces both human infections I_h(t) and infected mosquito populations I_m(t), in comparison to the uncontrolled scenario, where infection levels increase and saturate at high levels by the year 2030. Under this control strategy, the recovered human population R_h(t) is nearly eliminated due to the significant reduction in new infections. The control u_1(t) is applied at its maximum intensity from 2022 to 2026, after which it is gradually phased out. This suggests that a short-term, intensive prevention effort can effectively suppress malaria transmission. However, the presence of oscillations in I_m(t) suggests potential system instability, highlighting the need for continuous monitoring and possible supplementary interventions. Overall, while u_1(t) demonstrates strong potential as a standalone strategy, its long-term effectiveness may be limited without ……..

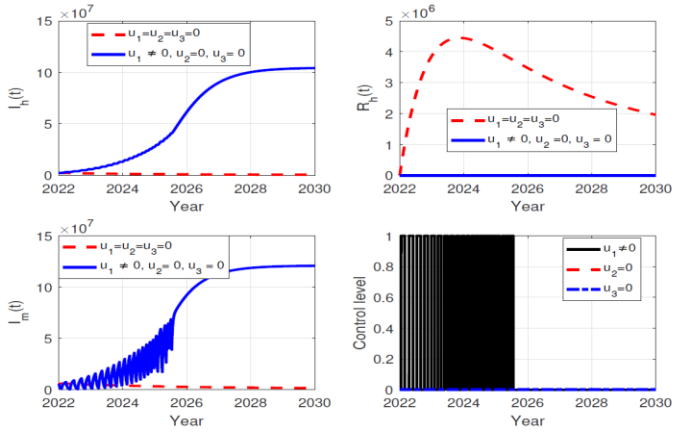


Figure 5: Simulations of the model showing the effect of $u_1(t)$ only on infected humans $I_h(t)$, recovered humans $R_h(t)$, infected mosquitoes $I_m(t)$ and the control profile respectively. Dashed red line represents system without optimal control ($u_1 = 0$, $u_2 = 0$, $u_3 = 0$) and solid blue line shows the system with optimal control ($u_1 \neq 0, u_2 = 0, u_3 = 0$).

Prevention of Malaria Through Treatment Control Only ($u_2(t)$)

Figure (6) presents the simulation results for the scenario in which only the treatment control $u_2(t)$ is activated, while the other controls are set to zero ($u_1(t) = u_3(t) = 0$). The results demonstrate that implementing $u_2(t)$ alone has minimal impact on the overall epidemic dynamics. The trajectory of human infections $I_h(t)$ under this control nearly coincides with the baseline (uncontrolled) scenario, exhibiting only a marginal improvement in the infection decay rate. Similarly, the recovered human population $R_h(t)$ and the infected mosquito population $I_m(t)$ show negligible differences between the controlled and uncontrolled cases.

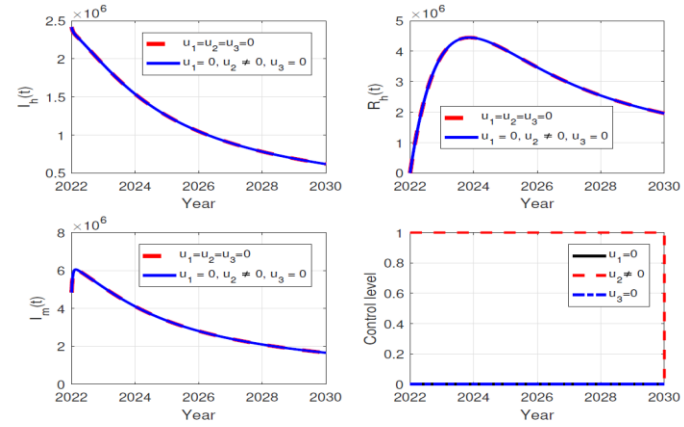


Figure 6: Simulations of the model showing the effect of u2(t) only on infected humans $I_h(t)$, recovered humans $R_h(t)$, infected mosquitoes $I_m(t)$ and the control profile respectively. The dashed red lines represent system without optimal control ($u_1 = 0$, $u_2 = 0$, $u_3 = 0$) and the solid blue lines show the system with optimal control ($u_1 = 0, u_2 \neq 0, u_3 = 0$).

Even though the control $u_2(t)$ is applied at its maximum intensity throughout the period 2022-2030, it fails to significantly reduce the burden of malaria in either the human or mosquito population. These findings suggest that $u_2(t)$, when used in isolation, targets a less influential transmission pathway or constitutes an intervention of limited effectiveness. In comparison to the earlier scenario involving $u_1(t)$, which demonstrated a substantial suppression of infections, the ineffectiveness of $u_2(t)$ underscores its limited utility as a standalone control measure. This raises important considerations regarding the cost-effectiveness and strategic value of treatment-focused interventions in malaria epidemic control planning.

Prevention of malaria through treatment ($u_3(t)$) only

Figure (7) explores the epidemiological response to activating only the control $u_3(t)$, with all other controls deactivated. The figure presents the dynamics of human infections $I_h(t)$, recoveries $R_h(t)$, infected mosquitoes $I_m(t)$, and the level of control application over time. As shown in the top-left panel of Figure (7), the application of $u_3(t)$ alone yields an unexpected outcome: rather than decreasing, the number of infected humans (blue solid line) exhibits a slight upward trend over time, diverging from the baseline scenario (red dashed line). This suggests a counterproductive effect. The top-right panel further supports this conclusion, where the recovery curve remains virtually flat at zero, indicating an absence of recoveries. This implies that human infections are either unresolved within the model or persist without recovery.

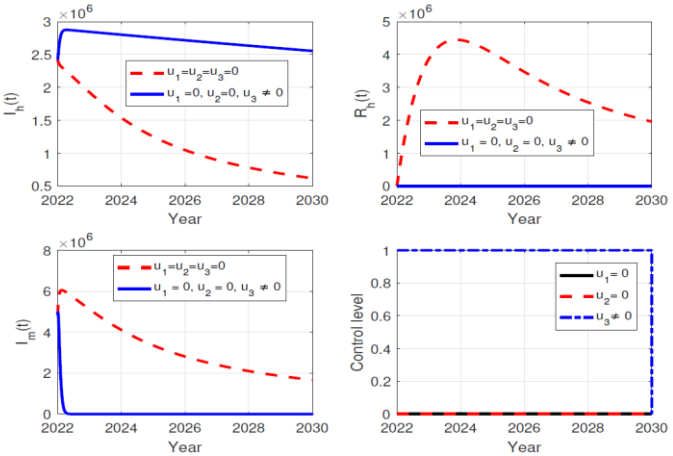


Figure 7: Simulations of the model showing the effect of $u_3(t)$ only on infected humans $I_h(t)$, recovered humans $R_h(t)$, infected mosquitoes $I_m(t)$ and the control profile respectively. Dashed red line represents system without optimal control ($u_1 = 0$, $u_2 = 0$, $u_3 = 0$) and solid blue line shows the system with optimal control ($u_1 = 0, u_2 = 0, u_3 \neq 0$)

This observation is consistent with the elevated levels of $I_m(t)$ and further confirms that $u_3(t)$ does not effectively reduce the human disease burden directly. In stark contrast, the bottom-left panel of Figure (7) shows that $I_m(t)$ experiences a rapid and sustained decline under the influence of $u_3(t)$, dropping to near-zero levels and remaining suppressed through 2030. This demonstrates that $u_3(t)$ is highly effective in targeting the mosquito infection compartment, successfully interrupting the transmission chain at that level. Finally, the bottom-right panel confirms the persistent, full-strength application of $u_3(t)$ throughout the entire simulation period, while controls $u_1(t)$ and $u_2(t)$ remain inactive, consistent with the scenario

setup. In summary, control $u_3(t)$ appears to be highly compartment-specific: it excels in suppressing $I_m(t)$ but is ineffective or potentially harmful in reducing human infections. These findings emphasize the necessity of integrated control strategies. While $u_3(t)$ may be valuable as part of a comprehensive, multipronged intervention, its isolated application may result in unintended negative consequences for human health.

Prevention of malaria using ($u_1(t)$) and ($u_2(t)$) controls

Figure (8) illustrates the epidemic trajectory when the first two controls, $u_1(t)$ and $u_2(t)$, are activated, while the third control, $u_3(t)$, remains inactive. In the top-left panel of Figure (8), the solid blue line exhibits a sharp and sustained decline in the number of infected humans $I_h(t)$, reaching near-zero levels by 2026. This contrasts with the uncontrolled trajectory (dashed red line), which shows only a gradual decline over time. Clearly, the combined control strategy is substantially more effective. The top right panel further supports this observation: the recovered human population $R_h(t)$ is notably suppressed under the control regime. The blue curve peaks early, followed by a steep decline, suggesting that fewer individuals progress to recovery because the control strategy prevents infection in the first place. This emphasizes that the intervention is primarily preventive rather than therapeutic. The lower-left panel of Figure (8) reveals that infections among intermediate hosts $I_m(t)$ undergo a rapid initial decline, followed by mild oscillations around very low levels. Although full stabilization is not achieved, the overall infection burden remains significantly lower than in the uncontrolled scenario. Additionally, the bottom-right panel shows that both $u_1(t)$ and $u_2(t)$ are maintained at full or near-full intensity throughout the simulation period, whereas $u_3(t)$ stays inactive, consistent with the experimental setup. This dual-control strategy demonstrates clear advantages over singular approaches. Specifically, it enables: (i) rapid suppression of human infections, nearly eliminating disease burden within a few years; (ii) sustained protection against resurgence, reflected by minimal recovery levels; and (iii) effective, though somewhat oscillatory, suppression of mosquito infections. In conclusion, the combination of $u_1(t)$ and $u_2(t)$ constitutes a robust and efficient control approach, outperforming isolated strategies. While the exclusion of $u_3(t)$ limits direct intervention in the intermediate host population, upstream suppression of human infections effectively disrupts transmission dynamics. These findings underscore the importance of integrated public health strategies that employ complementary interventions across multiple transmission pathways.

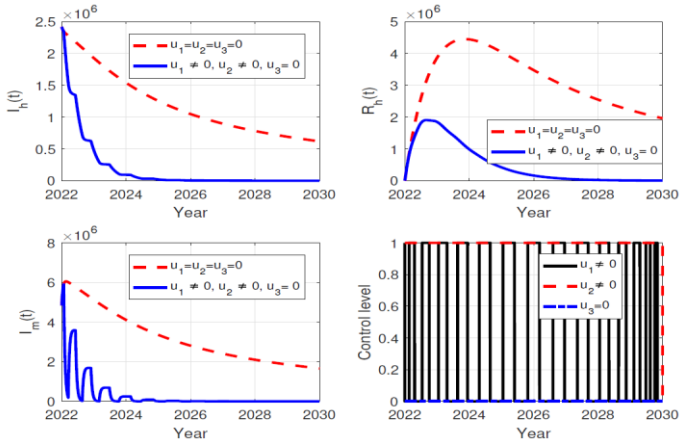


Figure 8: Simulations of the model showing the effect of $u_1(t)$ and $u_2(t)$ only on infected humans $I_h(t)$, recovered humans $R_h(t)$, infected mosquitoes $I_m(t)$ and the control profile respectively. Dashed red line represents system without optimal control (u_1=0, u_2 = 0, u_3 = 0) and solid blue line shows the system with optimal control ($u_1 \neq 0, u_2 \neq 0, u_3 = 0$).

Prevention of malaria using ($u_1(t)$) and ($u_3(t)$) controls

Figure (9) summarizes the epidemic dynamics under the combined action of controls $u_1(t)$ and $u_3(t)$, with no contribution from $u_2(t)$. The top-left panel shows that the infected human population $I_h(t)$ under this strategy (the solid blue line) exhibits stagnation or even a slight increase when compared to the uncontrolled scenario (the dashed red line). Although it might be expected that the combination of two controls would result in strong suppression of infections, this outcome suggests a non-additive or possibly antagonistic interaction between $u_1(t)$ and $u_3(t)$. Moreover, as shown in the top-right panel, the recovery curve remains close to zero throughout the simulation window. This either indicates effective prevention of new infections or reflects minimal recovery due to persistently low disease resolution, consistent with suppressed but ongoing transmission. The lower-left panel illustrates a dramatic reduction in the mosquito infection population $I_m(t)$, which drops to nearly zero shortly after the simulation begins. This aligns with previous findings that identified $u_3(t)$ as highly effective in targeting intermediate reservoirs. The addition of $u_1(t)$ does not appear to enhance this suppression, likely because $u_3(t)$ alone already achieved near-elimination in earlier scenarios. Finally, the bottom-right panel confirms that both $u_1(t)$ (the black line) and $u_3(t)$ (the blue dashed line) are applied at full strength throughout the control window, while $u_2(t)$ remains inactive. The consistent, steady state application indicates a fixed control policy rather than an adaptive or feedback-based approach. In summary, the combined application of $u_1(t)$ and $u_3(t)$ demonstrates strong compartment-specific effects particularly in reducing $I_m(t)$ but fails to significantly suppress human infections. This highlights the importance of strategic control pairing and the potential pitfalls of assuming additive benefits from combining interventions without considering their interactions.

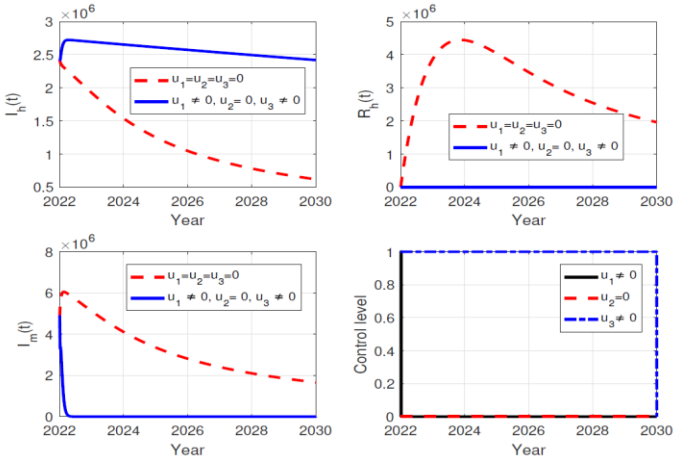


Figure 9: Simulations of the model showing the effect of $u_1(t)$ and $u_3(t)$ only on infected humans $I_h(t)$, recovered humans $R_h(t)$, infected mosquitoes $I_m(t)$ and the control profile respectively. Dashed red line represents system without optimal control (u_1=0, u_2 = 0, u_3 = 0) and solid blue line shows the system with optimal control ($u_1 \neq 0, u_2 = 0, u_3 \neq 0$).

Prevention of malaria using ($u_2(t)$) and ($u_3(t)$) controls

Figure (10) presents the epidemic outcomes under the combined application of controls $u_2(t)$ and $u_3(t)$, with the human-directed control $u_1(t)$ remaining inactive. This scenario is designed to assess whether indirect and ecological interventions can compensate for the absence of direct public health measures. In the top-left panel, the effect on human infections, $I_h(t)$ is striking: the controlled trajectory (solid blue line) drops sharply after 2022, reaching near-zero levels by 2025. This decline is significantly steeper than that observed in the uncontrolled case (dashed red line), indicating a robust suppressive effect despite the absence of direct treatment or vaccination. This result is notable, given that $u_2(t)$ and $u_3(t)$ were previously shown to be weakly effective when applied individually. Their combined effect, however, reveals a synergistic interaction that yields an emergent benefit. The top-right panel supports this observation. The trajectory of recovered individuals $R_h(t)$ (the blue curve) peaks early and then rapidly declines toward zero by the middle of the decade. This pattern suggests that very few individuals progress to the recovered state, likely due to early interruption of transmission rather than progression through the disease. The implication is that the control strategy is not merely reducing disease severity or duration but is effectively preventing infections from occurring in the first place. In the lower-left panel, mosquito infections $I_m(t)$ collapse in a similarly rapid fashion, approaching zero within the first two years of the simulation. This outcome confirms the high efficacy of $u_3(t)$ in disrupting transmission among intermediate hosts. The presence of $u_2(t)$ may enhance this effect by promoting behavioral or environmental changes that reduce contact rates between humans and mosquitoes or minimize contamination. The bottom-right panel illustrates the temporal profiles of the applied controls. Both $u_2(t)$ (the red dashed line) and $u_3(t)$ (the blue dotted line) are initially deployed at full intensity, then gradually taper off after 2028. This pattern indicates a transition toward endemic control or possible eradication; wherein sustained intervention is no longer necessary once transmission falls below critical thresholds. Overall, the combination of $u_2(t)$ and $u_3(t)$ demonstrates the potential for non-human-targeted interventions to achieve substantial epidemic suppression, especially when applied synergistically. This highlights the importance of considering ecological and behavioral controls as viable components of integrated disease management strategies.

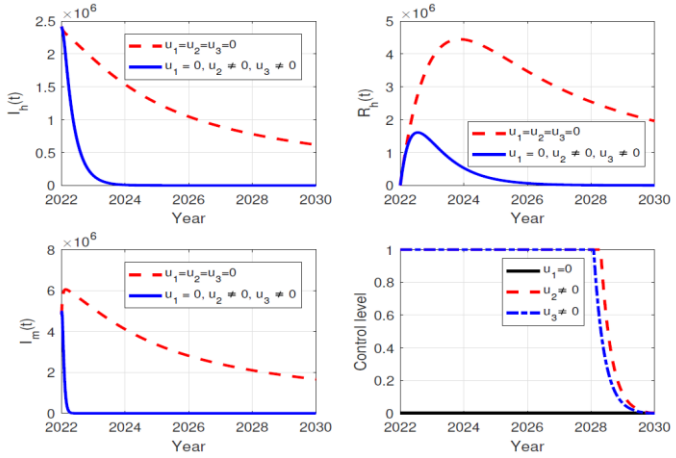


Figure 10: Simulations of the model showing the effect of $u_1(t)$ and $u_3(t)$ only on infected humans $I_h(t)$, recovered humans Rh(t) , infected mosquitoes $I_m(t)$ and the control profile respectively. The dashed red line represents system without optimal control (u_1=0, u_2 = 0, u_3 = 0) and the solid blue line shows the system with optimal control ($u_1 = 0, u_2 \neq 0, u_3 \neq 0$).

Prevention of Malaria Using Controls $u_1(t)$, $u_2(t)$, and $u_3(t)$

Figure (11) illustrates the epidemic outcomes when the full set of control interventions is simultaneously applied. In the top-left subplot of Figure (11), we observe the most aggressive suppression of human infections across all considered scenarios. The blue line, representing the controlled system, shows a steep decline in $I_h(t)$ within the first two years, followed by sustained near-zero infection levels through 2030. This indicates early eradication of human transmission due to the comprehensive effect of all three controls. The top-right panel of Figure (11) shows that the recovered human population Rh(t) peaks early and then rapidly declines to near-zero. The behavior of the blue curve confirms that most potential infections are prevented altogether rather than simply mitigated or resolved, thereby avoiding a significant buildup of recovered individuals. This underscores the preventive power of the full-control regime. As depicted in the bottom left panel of Figure (11), mosquito infections $I_m(t)$ also collapse within the first few years, mirroring the human infection trend. The suppression is both rapid and stable, without the oscillatory behavior observed in some single-control scenarios, indicating enhanced system stability when all three controls act in synergy. The bottom-right panel displays the trajectories of the control functions. Each of $u_1(t)$, $u_2(t)$, and $u_3(t)$ begin at full intensity (value of 1) and then gradually tapers off around 2028. This coordinated decline suggests a natural phasing-out of interventions as the system approaches a stable,

disease-free equilibrium. The uniform tapering across all controls indicates that the system has reached a point where continued intervention is no longer necessary, a desirable feature in long-term public health policy. Overall, the full-control scenario yields the optimal outcome across all dimensions: human infections are rapidly and sustainably eliminated; the recovery burden is minimized through effective prevention; and mosquito infections are extinguished. Furthermore, although the control efforts are initially intensive, they are time-limited, ending naturally as the epidemic subsides.

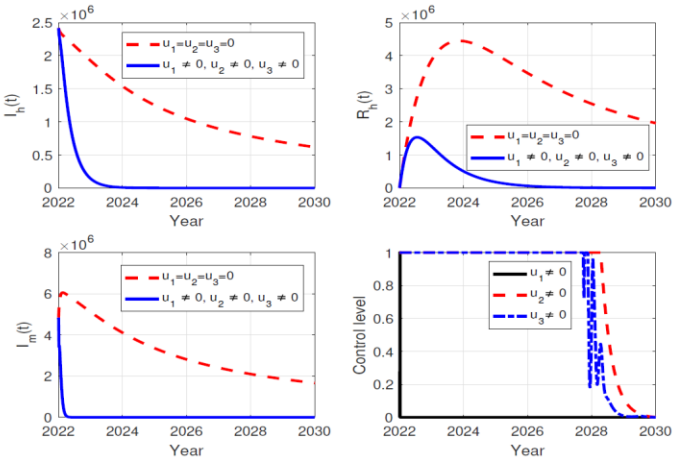


Figure 11: Simulations of the model showing the effect of $u_1(t)$ and $u_3(t)$ only on infected humans $I_h(t)$, recovered humans $R_h(t)$, infected mosquitoes $I_m(t)$ and the control profile respectively. The dashed red line represents the system without optimal control ($u_1=0$, $u_2 = 0$, $u_3 = 0$) and solid blue line shows the system with optimal control ($u_1 \neq 0, u_2 \neq 0, u_3 \neq 0$).

The comprehensive intervention utilizing all three controls $u_1(t)$, $u_2(t)$, and $u_3(t)$ offers a robust solution for epidemic containment and elimination. It harnesses the strengths of each control strategy, offsets their individual limitations, and supports the eventual withdrawal of interventions. These results strongly advocate for the use of integrated, multi-targeted public health strategies to achieve sustainable epidemic control.

7. DISCUSSION

The backward bifurcation identified analytically in Section 3 and numerically in Table 1 is consistent with earlier malaria and vector-borne disease models that incorporate re-infection or incomplete immunity, such as Xiaomei Feng, et al. [8], Danbaba, et al. [14], and Kelatlhegile and Kgosimore [15], all reported multiple endemic equilibria coexisting with a stable disease-free equilibrium when R0 < 1. This reinforces the conclusion that, in settings such as the DRC where partial immunity and re-infection are epidemiologically relevant, driving R0 below unity is a necessary but not always sufficient condition for elimination; control strategies must also reduce the initial infective load below the unstable threshold associated with the smaller endemic equilibrium.

Our finding that combined, multi-pathway control ($u_1 + u_2 + u_3$) substantially outperforms any single or paired intervention is consistent with the general conclusions of Liming Cai, et al. [10] and Adepoju and Olaniyi [16], who likewise found that single-intervention strategies (treatment-only or vertical-transmission-blocking alone) provide only partial epidemic control. It is also consistent with the DRC-specific burden assessment of Deutsch-Feldman, et al. **[1]**, who emphasize that the scale of DRC's malaria burden requires layered interventions rather than single-modality programs.

Generalizability: Because the loss-of-immunity rate ρ, recovery rate α, and re-infection probability δ were fitted specifically to DRC cumulative case data, the quantitative eradication timelines reported in Section 6 should not be directly extrapolated to countries with substantially different transmission intensity, mosquito species composition, health-system capacity, or baseline intervention coverage. The qualitative findings—the existence of backward bifurcation and the superiority of combined controls—are structural properties of the model and are expected to generalize, but the specific parameter values and projected timeframes are DRC-specific.

Assumptions and limitations: The model assumes constant human and mosquito population sizes and that mosquitoes do not recover once infected. The constant-population assumption neglects disease-induced or demographic changes in population size over a multi-year horizon; relaxing it (e.g., allowing birth/death imbalance or disease-induced mortality) would be expected to slow, but not qualitatively reverse, the projected decline in infections under the full-control scenario, since the mechanism driving eradication in Section 6 is the suppression of transmission rather than population attrition. Similarly, the assumption that mosquitoes do not recover is conservative with respect to control effectiveness: allowing mosquito recovery would tend to lengthen, rather than shorten, the time to elimination. We therefore consider the reported "eradication within a few years" outcome to be an optimistic but structurally robust upper bound on intervention effectiveness, rather than a precise operational forecast.

8. CONCLUSION

A malaria transmission model, specifically tailored to the Democratic Republic of Congo, has been developed to capture the effects of partial immunity and re-infection dynamics within the human population. Analytical investigations confirm the presence of a backward bifurcation, indicating that reducing the basic reproduction number, R_0, below unity is not necessarily sufficient for disease elimination. Sensitivity analysis identifies key transmission parameters, thereby providing strategic targets for intervention. The optimal control analysis demonstrates that, while individual measures such as bed-net usage, $u_1(t)$, antimalarial treatment, $u_2(t)$, or insecticide spraying, $u_3(t)$, can reduce infection prevalence, their impacts remain limited or compartment-specific when implemented in isolation. In contrast, the combined application of all three interventions results in rapid and sustained declines in both human and mosquito infections, with numerical simulations suggesting the possibility of eradication within a short period. These results emphasize the necessity of coordinated, multi-pathway control strategies for effective malaria elimination. The proposed model serves as a valuable decision-support tool for policymakers, facilitating evidence-based resource allocation and the design of efficient, region-specific malaria control programs in the DRC.

9. REFERENCES

[1] Deutsch-Feldman, Molly, et al. "The burden of malaria in the Democratic Republic of the Congo." The Journal of Infectious Diseases 223.11 (2021): 1948-1952.

[2] Oladipo, Habeebullah Jayeola, et al. " Increasing challenges of malaria control in sub-Saharan Africa: Priorities for public health research and policymakers." Annals of Medicine and Surgery 81 (2022): 104366.

[3] Venkatesan, Priya. " The 2023 WHO World malaria report." The Lancet Microbe 5.3 (2024): e214.

[4] NUNDU, SABITI SABIN. " Epidemiology of Plasmodium spp. infections among school-age children living in rural and urban areas of Kinshasa in Democratic Republic of Congo." (2022).

infection in mosquitoes." Mathematics 10.21 (2022): 3950.

[5] Eikenberry, Steffen E., and Abba B. Gumel. " Mathematical modeling of climate change and malaria transmission dynamics: a historical review." Journal of mathematical biology 77.4 (2018): 857-933.

[6] Rajnarayanan, Adithya, Manoj Kumar, and Abdessamad Tridane. " Analysis of a mathematical model for malaria using data-driven approach." Scientific Reports 15.1 (2025): 27272.

[7] B.Edoardo and etal, A mathematical model for malaria transmission with asymptomatic carriers and two age groups in the human population. Mathematical Biosciences, 300 (2018), 87-101, DOI:10.1016/j.mbs.2018.03.024.

[8] X. Feng et al. Stability and backward bifurcation in a malaria transmission model with applications to the control of malaria in China. Mathematical Biosciences 266 (2015) 52-64.

[9] S. Kim et al. Analysis of a vector-bias effect in the spread of malaria between two different incidence areas.Journal of Theoretical Biology 419 (2017) 66-76.

[10] Liming Cai et al. Optimal control of a malaria model with asymptomatic class and superinfection. Mathematical Biosciences (2017), DOI:10.1016/j.mbs.2017.03.003

[11] Supriatna, Asep K., et al. " Age-dependent survival rates in SIR-SI dengue transmission model and its application considering human vaccination and Wolbachia

[12] Saha, Amit Kumar, Shikha Saha, and Chandra Nath Podder. " Optimal control and cost-effectiveness analysis of a fractional order drug-resistant malaria transmission model with recovered carriers." medRxiv (2025): 2025-05.

[13] Sharon, A. Okwomi, et al. " Bayesian reasoning and SIR malaria models." Commun. Math. Biol. Neurosci. 2025 (2025): Article-ID.

[14] Danbaba, U. A., M. D. Aloko, and A. M. Ayinde. " Mathematical modeling of mosquito borne diseases with vertical transmissions as applied to Dengue." International Journal of Mathematical Sciences and Optimization: Theory and Applications 10.3 (2024): 31-56.

[15] G.R. Kelatlhegile, M. Kgosimore.Bifurcation analysis of vertical transmission model with preventive strategy.Journal of the Egyptian Mathematical Society (2016) 24, 492-498.

[16] Adepoju, Okunloye A., and Samson Olaniyi. " Stability and optimal control of a disease model with vertical transmission and saturated incidence." Scientific African 12 (2021): e00800.

[17] J.Wang and et al. The backward bifurcation of a model for malaria infection. International Journal of Biomathematics Vol.11,NO.2(2018) 1850018(18pages).

[18] W. Hirsch, H. Hanisch, J. Gabril, Differential equation models of some parasitic infections: methods for the study of asymptotic behavior, Commun. Pure. Appl. Math., 38(1985)733-753.

[19] Van den Driessche P, Watmough J. Reproduction numbers and sub-threshold endemic equilibria for compartmental models of disease transmission. Mathematical Biosciences. 2002;180:29-48.

[20] David R. Merkin. Introduction to the Theory of Stability. Springer-Verlag, New York, 1997.

[21] C. Castillo-Chavez and B.Song. Dynamical models of Tuberculosis and their applications.

[22] M. Kot. Elements of Mathematical Ecology, Cambridge University

Press, Cambridge, 2001.

[23] Available at:http://apps.who.int/gho/data/

r

[24] Available at:http:www.who.int/malaria/publications/world-malaria - report- 2017/en/

[25] CDC, Anopheles Mosquitoes. Centers for Disease Control and Prevention, 2015.

[26] Available at:https://knoema.com/atlas/Democratic-Republic-of-the- Congo/topics/Demographics/Population-forecast/Life-expectancy

[27] N. Chitnis, J. Hyman, J. Cushing, Determining Important Parameters in the Spread of Malaria Through the Sensitivity Analysis of a Mathematical Model. Bull. Math. Biol., 70 (2008) 1272-1296.

[28] Folashade B. Agusto et al. Application of Optimal Control to Epidemiology of Malaria. Electronic Journal of Differential Equations,Vol.(2012), No.81, pp.1-22.

[29] Fleming WH, Rishel RW. Deterministic and Stochastic Optimal Control. Springer-Verlag, New York, 1975.